Original Paper

phys. stat. sol. (b) **244**, No. 11, 4275–4278 (2007) / **DOI** 10.1002/pssb.200776121

Detail study of the Raman-active modes in carbon nanotubes

M. Mohr[*, 1], **M. Machón**[1], **C. Thomsen**[1], **I. Milošević**[2], and **M. Damnjanović**[2]

[1] Institut für Festkörperphysik, Technische Universität Berlin, Hardenbergstr. 36, 10623 Berlin, Germany
[2] Faculty of Physics, University of Belgrade, P.O. Box 368, 11011 Belgrade, Serbia

Received 14 May 2007, revised 27 July 2007, accepted 27 July 2007
Published online 26 September 2007

PACS 61.46.Fg, 63.20.Kr, 63.20.Ry, 71.15.Mb, 78.30.Na

The Raman-active A_1-modes in carbon nanotubes are often used for characterizing nanotube samples. The fully-symmetric radial-breathing mode and the high-energy mode (HEM) have small non-radial and non-tangential components, respectively. Neglecting these components results in errors for phonon frequency and electron–phonon coupling calculations. We present a model to estimate these non-radial components. For the HEM we find an anharmonicity that stems from the three-fold coordination of the C atoms.

The Raman spectrum of nanotubes (NTs) is dominated by the fully symmetric modes [1, 2]. These modes are the low-energy radial breathing mode (RBM) and two high-energy modes (HEMs), derived from the E_{2g}-mode of graphene. In achiral tubes due to mirror planes, one of these HEMs becomes odd and is Raman-forbidden. With the help of the RBM the diameter of nanotubes can be identified; its diameter dependent frequency can be compared to calculated frequencies. With resonant Raman scattering the chiral indices (n,m) were identified [3]. Efforts have been made to estimate chiral abundancies of nanotubes in solution from the intensity in Raman experiments [4]. For this, a detailed knowledge of the Raman cross section is necessary. It has been shown that it depends not only on excitation energy but also on chirality with tight-binding and density functional theory calculations [5, 6]. Even small diameter tubes can have several hundreds of atoms in a unit cell, thus making DFT calculations very expensive. The fact that the optical resonance is governed by excitons [7, 8] makes the description in one-particle DFT even harder and extensions have to be used. The use of valid approximations is therefore extremely helpful and speeds up the calculations.

In contrast to other authors who make use of the force-constant matrix, e.g., Ref. [9], we apply a different model to find the phonon eigenvector. Our variational model is adopted from Ref. [10] and applied to entire nanotubes. It is based on the idea that an atomic displacement increases the total energy of the SWNT. If we displace all atoms according to a pattern that corresponds to an irreducible representation, the direction with extremal energy values reflects a phonon mode with this irreducible representation. This has been successfully done to obtain phonon modes in benzene [11]. Technically, we displace one atom freely on a sphere with fixed radius. Then we apply the symmetry operations that are used to construct a nanotube [1] to the displacement vector and calculate the total energy of this displaced system with the DFT-code SIESTA [12, 13]. We use the LDA functional in the parametrization of Perdew and Zunger [14] and Troullier–Martins [15] pseudopotentials. For the real space grid integrations an equivalent energy cutoff of 270 Ry was used and 16 k-points along the nanotube axis in reciprocal space. The valence electrons were described by a double-ζ basis set with cutoff radii of 5.12 bohr and 6.25 bohr for the s and p orbitals, respectively plus an additional polarizing orbital. The ground state was obtained from relaxing all atoms until all forces were below 0.01 eV/Å.

* Corresponding author: e-mail: marcel@physik.tu-berlin.de

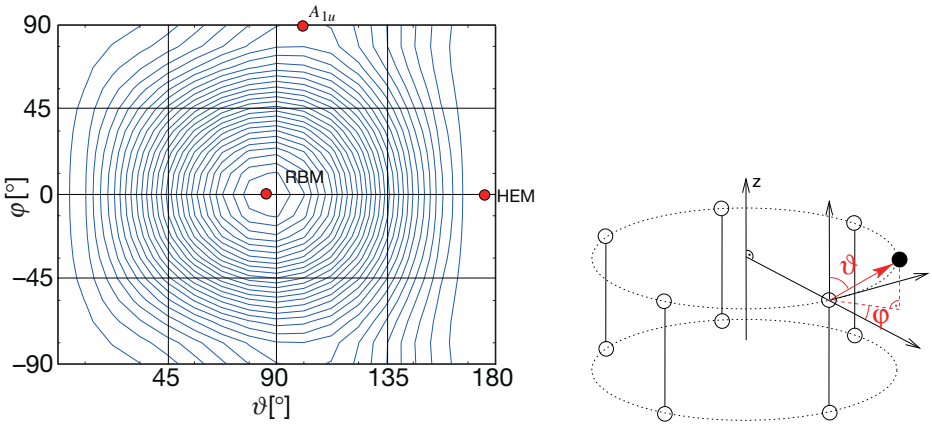

Fig. 1 (online colour at: www.pss-b.com) Left: Total energy contour plot of the (5,0)-nanotube as a function of ϑ and φ. Fully symmetric eigenmodes are in the directions of extremal total energy. Note the mirror symmetry at $\varphi = 0°$ corresponding to the mirror plane in zigzag (n,0) NTs. Right: Section of a (5,0)-NT to illustrate the angles ϑ and φ.

A typical result is shown in Fig. 1, where we present an energy-contour plot of a (5,0)-tube for atomic displacements within a half-sphere; the definition of ϑ and φ is illustrated on the right side of Fig. 1. We find a minimum and two saddle points. We assign the minimum and one saddle point to A_{1g}-modes, the RBM and the HEM, respectively. The second saddle point corresponds to a A_{1u}-mode. In chiral tubes, due to the lack of mirror planes, there is no distinction between even (g) and odd (u) modes, and both saddle points correspond to a fully symmetric A_1-modes.

The eigenvector of the RBM for general NTs is not exactly radial ($\vartheta = 0°$, $\varphi = 0°$) but slightly displaced. Due to symmetry, we find for zigzag NTs $\varphi = 0°$, while for armchair we have $\vartheta = 0°$. Values obtained for ϑ and φ for several NTs can be found in Ref. [16]. For the HEM we also find non-tangential components for all nanotubes. The deviation from a tangential plane is of similar size, i.e., up to a few degrees for small diameter tubes. These results verify findings from finite differences calculations [9].

A closer look at Fig. 1 reveals that the energies at $\vartheta = 0°$ and 180° are not exactly equal. However within a harmonic approximation this is expected. *Ab initio* calculations for the E_{2g}-mode in graphene show also differing energies at positive and negative displacements for the corresponding direction. This is a consequence of the three-fold geometry. To show this we use a simple model that only considers bond-stretching interaction between nearest neighbors. In an E_{2g}-mode of graphene neighboring atoms move in

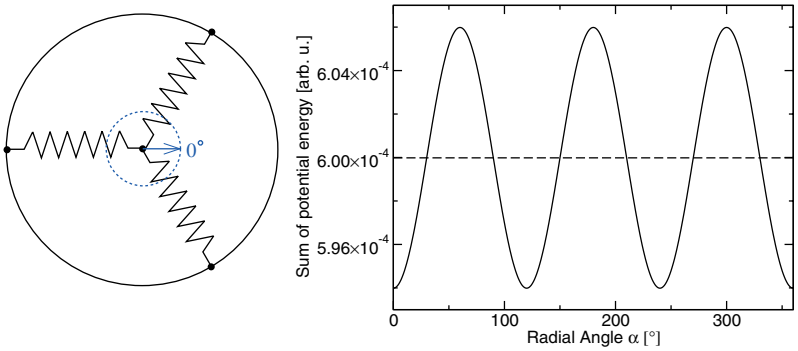

Fig. 2 (online colour at: www.pss-b.com) Left: Three-spring model. Right: Sum of potential energy for the radial displacement as shown in left figure.

opposite directions [17]. If we fix the three neighbors and only move the central atom, we obtain the same relative distances than in an E_{2g}-mode. The central atom (see Fig. 2) is attached to its neighbors with springs. On the right side of Fig. 2 we plot the potential energy of the three springs as function of the radial angle α ($\alpha = 0°$ is indicated on the left side of Fig. 2). Only for values of $\alpha = 30°$, 90° and 150° the potential energies at the positive (α) and negative displacement ($\alpha + 180°$) are equal. This is in agreement with all mirror-planes and the three-fold rotation. For all other values of α the potential energy at positive and negative displacements differ. For a displacement of 2% of the nearest-neighbor distance, we find a relative difference in potential energy of 2% between the maximum and the minimum which is of similar magnitude as the relative energies at $\vartheta = 0°$ and 180°.

This anharmonicity does not seem to have an effect on the phonon frequencies. Within the frozen phonon approximation, the frequency is obtained from the quadratic coefficient of the potential energy versus the displacement [18]. A fit of the energy versus displacement for $\alpha = 90°$ is perfectly harmonic. A 3rd order fit for $\alpha = 0°$ leads to non-zero values for the linear and cubic coefficients, but to the same quadratic coefficient as for $\alpha = 90°$, and thus yields the same phonon frequency. As the common methods for phonon calculations, finite differences or linear response, use the harmonic approximation to obtain the phonon frequency, this effect could not be detected.

The non-radial components have an influence on the electron–phonon coupling strengths for the RBM [6]. We compare the deformation potential $\partial E_{kn}/\partial Q_\alpha$ for the non-mixed and mixed displacement patterns. From the deformation potentials $\partial E_{kn}/\partial Q_\alpha$ the matrix elements $\mathcal{M}_i$ can be obtained (details and definitions can be found in Refs. [6] and [19]). We find an increase of $\partial E_{kn}/\partial Q_\alpha$ for the non-mixed displacement pattern between 30% and 60%. As the observed Raman intensity is proportional to the square of the matrix elements $\mathcal{M}_i$, the mixed eigenvectors yield systematically smaller Raman signals. For semiconducting zigzag tubes, the average of the matrix elements increases by a factor of 1.5, whereas for metallic zigzag tubes (15,0) we find an increase of 30%. For armchair tubes we find an increase of 1.3 to 1.4. Details can be found in Ref. [16]. The influence of the mixing on the HEM is smaller. The matrix elements of the non-mixed HEM do not show any detectable difference for zigzag tubes, whereas the matrix elements for armchair increase by 4% to 7%.

To analyze the effect of these components on the calculation of phonon frequencies we use a frozen-phonon approach [18] for the purely radial displacement. We compare these frequencies with values obtained *via* finite-differences calculations [6] that include a mixing. In Fig. 3 we show the calculated frequencies in both cases. Neglecting the non-radial components results in errors of up to 10 cm^{-1} in agreement with Ref. [20]. As stated in Ref. [21] a fine structure can be identified. Diameter-corrected,

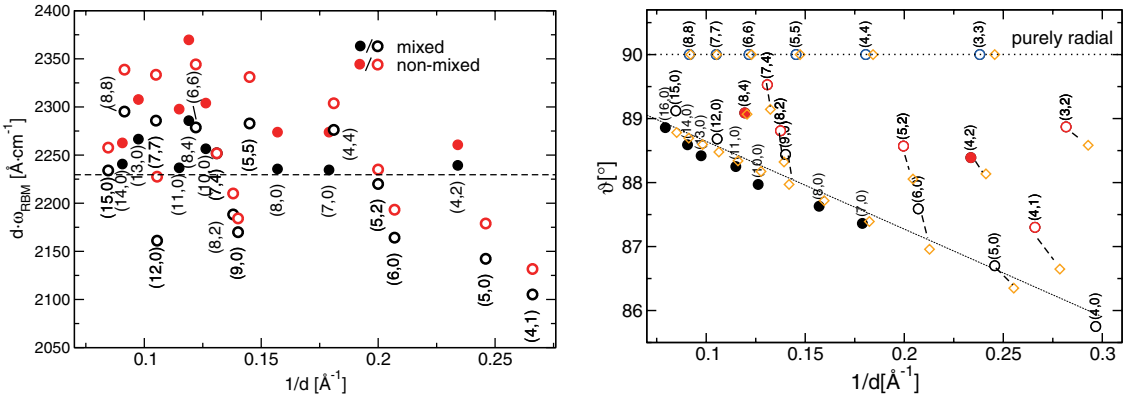

Fig. 3 (online colour at: www.pss-b.com) Left: Frequency ω_{RBM} times diameter for the RBM calculated for the eigenvector (mixed) and the pure radial displacement (non-mixed). Right: Angle ϑ of the RBM versus the inverse diameter $1/d$ for several NTs, obtained from the minimum of the total energy (circles) and from our graphene-model (diamonds) of Eq. (1). Open circles denote metallic tubes.

armchair NTs have the highest frequencies, zigzag tubes the lowest frequencies. This is an effect of the geometry as a molecular mechanic model shows [22]. Additionally, the frequency of metallic tubes is smaller than that of similar semiconducting tubes. For the HEM of metallic tubes we observe the well-known phonon softening [9] related to the Kohn-anomaly at the Fermi point.

After we have shown that these small components have large effects, we turn our attention to how we can incorporate them into future calculations. Considering the atomic forces for the radial displacement we find smallest tangential components of the atomic force for the eigenvector of the RBM. We use this observation to estimate the nonradial components of the RBM from graphene. Stretching the unit cell of graphene according to a RBM-like pattern results in HEM-like forces. Equating these forces with those of a HEM-like displacement gives the appropriate mixing. We find for a change in tube radius Δr

$$\frac{\Delta z}{\Delta r} = \frac{2\pi}{19.7\sqrt{n^2+m^2+nm}} \cos(3\theta) \quad \text{and} \quad \frac{\Delta y}{\Delta r} = \frac{2\pi}{16.7\sqrt{n^2+m^2+nm}} \sin(3\theta), \tag{1}$$

where $\Delta z/\Delta r = \tan(90° - \vartheta)$ and $\Delta y/\Delta r = \tan\varphi$. n, m are the chiral indices of a (n,m)-tube. For achiral tubes we obtain good agreement. For chiral tubes the components are overestimated, but still remain a good approximation. These data points we plot on the right side of Fig. 3.

In this paper we discussed the mixing of the fully-symmetric modes. We showed that the RBM and the HEM have small non-radial and non-tangential components, respectively. We discussed the influence of these small components on the calculation of phonon frequencies and electron–phonon coupling and estimated the non-radial components of the RBM for all tubes. We found an anharmonicity for the HEM in NTs and the E_{2g}-mode in graphene.

Acknowledgement The authors acknowledge useful discussions with J. Maultzsch.

References

[1] M. Damnjanović, I. Milošević, T. Vuković, and R. Sredanović, Phys. Rev. B **60**(4), 2728 (1999).
[2] S. Reich, C. Thomsen, and J. Maultzsch, Carbon Nanotubes: Basic Concepts and Physical Properties (Wiley-VCH, Berlin, 2004).
[3] H. Telg, J. Maultzsch, S. Reich, F. Hennrich, and C. Thomsen, Phys. Rev. Lett. **93**, 177401 (2004).
[4] A. Jorio, A. P. Santos, H. B. Ribeiro, C. Fantini, M. Souza, J. P. M. Vieira, C. A. Furtado, J. Jiang, R. Saito, L. Balzano, D. E. Resasco, and M. A. Pimenta, Phys. Rev. B **72**, 075207 (2005).
[5] V. N. Popov, L. Henrard, and P. Lambin, Nano Lett. **4**(9), 1795 (2004).
[6] M. Machón, S. Reich, H. Telg, J. Maultzsch, P. Ordejón, and C. Thomsen, Phys. Rev. B **71**, 035416 (2005).
[7] F. Wang, G. Dukovic, L. E. Brus, and T. F. Heinz, Science **308**(5723), 838 (2005).
[8] J. Maultzsch, R. Pomraenke, S. Reich, E. Chang, D. Prezzi, A. Ruini, E. Molinari, M. S. Strano, C. Thomsen, and C. Lienau, Phys. Rev. B **72**, 241402(R) (2005).
[9] O. Dubay and G. Kresse, Phys. Rev. B **67**(3), 035401 (2003).
[10] M. Damnjanović, E. Dobardžić, and I. Milošević, J. Phys.: Condens. Matter **16**, L505 (2004).
[11] G. Sun, J. Kürti, P. Rajczy, M. Kertesz, J. Hafner, and G. Kresse, J. Mol. Struct. (Theochem.) **624**, 37 (2003).
[12] P. Ordejón, E. Artacho, and J. M. Soler, Phys. Rev. B **53**, R10441 (1996).
[13] J. M. Soler, E. Artacho, J. D. Gale, A. García, J. Junquera, P. Ordejón, and D. Sánchez-Portal, J. Phys.: Condens. Matter **14**, 2745 (2002).
[14] J. P. Perdew and A. Zunger, Phys. Rev. B **23**, 5048 (1981).
[15] N. Troullier and J. L. Martins, Phys. Rev. B **43**, 1993 (1991).
[16] M. Mohr, M. Machón, C. Thomsen, I. Milošević, and M. Damnjanović, Phys. Rev. B **75**, 195401 (2007).
[17] M. Mohr, J. Maultzsch, E. Dobardžić, S. Reich, I. Milošević, M. Damnjanović, A. Bosak, M. Krisch, and C. Thomsen, Phys. Rev. B **76**, 035439 (2007).
[18] M. T. Yin and M. L. Cohen, Phys. Rev. B **26**(6), 3259 (1982).
[19] M. Machón, S. Reich, and C. Thomsen, phys. stat. sol. (b) **243**(13), 3166 (2006).
[20] I. Milošević, E. Dobardžić, and M. Damnjanović, Phys. Rev. B **72**, 085426 (2005).
[21] J. Kürti, V. Zólyomi, M. Kertesz, G. Sun, R. H. Baughman, and H. Kuzmany, Carbon **42**, 971 (2004).
[22] T. Chang, Acta Mech. Sin. **23**(2), 159 (2007).

